Numerical and experimental study of the dynamics of axisymmetric slender liquid bridges

By JOSÉ MESEGUER AND ANGEL SANZ

Laboratorio de Aerodinámica, E.T.S.I. Aeronáuticos, Universidad Politécnica, 28040 Madrid, Spain

(Received 2 November 1983 and in revised form 12 October 1984)

A one-dimensional inviscid slice model has been used to study numerically the influence of axial microgravity on the breaking of liquid bridges having a volume close to that of gravitationless minimum volume stability limit. Equilibrium shapes and stability limits have been obtained as well as the dependence of the volume of the two drops formed after breaking on both the length and the volume of the liquid bridge. The breaking process has also been studied experimentally. Good agreement has been found between theory and experiment for neutrally buoyant systems.

1. Introduction

A number of recently published papers deal with the floating zone problem through idealized models in which, generally, phase changes are avoided. The most used model consists of a liquid bridge, either under gravitationless conditions or subject to a small axial gravity, held by surface tension forces between two parallel disks with a common axis (figure 1). Besides the analytical and experimental approaches made on thermal problems (mainly on Marangoni convection), the liquid bridge problem has received attention from many investigators: the shapes and static stability of liquid bridges at rest under gravitationless conditions have been studied by Haynes (1970), Erle, Gillette & Dyson (1970), Gillette & Dyson (1971), Martinez (1976), Da Riva & Martinez (1979), Slobozhanin (1982), Martinez (1983), Meseguer (1984), among others. The influence of microgravity or disks rotation (or both) have been considered by Coriell & Cordes (1977), Coriell, Hardy & Cordes (1977), Martinez (1978*a*, *b*), Boucher & Evans (1980), Brown & Scriven (1980), Da Riva (1981), Ungar & Brown (1982), and Vega & Perales (1983) among others. In addition, attempts have been made to solve some aspects of the dynamics of liquid bridges: the spin-up from rest has been considered in Da Riva & Meseguer (1978) and Da Riva & Manzano (1981), while the steady problem of a liquid bridge with disks rotating at different velocities was examined by Harriot & Brown (1983), and the breaking problem has been treated by Meseguer (1983*a*, *b*), Meseguer, Sanz & Rivas (1983) and Rivas & Meseguer (1984).

In this paper the influence of axial microgravity on the minimum volume stability limit of non-cylindrical liquid bridges is studied numerically from a dynamic point of view. The method is used to calculate the static characteristics of the liquid bridge, such as the equilibrium shapes and the minimum volume stability limit, and overall dynamic characteristics of the breaking process, i.e. the influence of axial microgravity, the length of the liquid bridge, and the volume of the liquid column on the volume of the two caps resulting after liquid bridge breaking. Characteristics of the breaking process are required to evaluate the ability of the slice model to predict the behaviour of axisymmetric slender liquid bridges. Numerical results shown in Meseguer

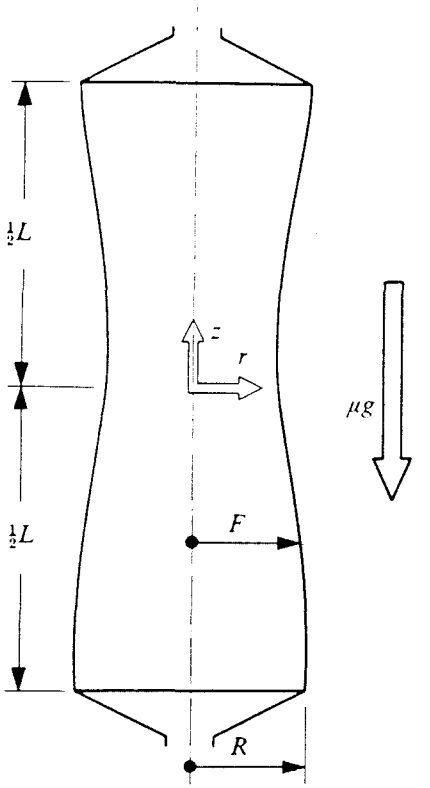

FIGURE 1. Geometry and coordinate system for the liquid bridge problem.

(1983*a*, *b*), Meseguer *et al.* (1983) and in this paper suggest that the volume of the caps mainly depends on both the length and the whole volume of the liquid bridge and not on the initial perturbation of the interface (provided these perturbations are small enough). Cap volume measurements have been used to compare theory with experiments.

From the experimental point of view the studies of liquid bridges carried out in earth-based laboratories are strongly constricted because the maximum stable length of a liquid bridge is of the order of a few millimetres. Slender liquid bridges can only be obtained by working on a very small scale, or by simulating microgravity conditions by using the neutral buoyancy with one liquid surrounded by a second with which it is immiscible but of precisely the same density. Neutral buoyancy has been used by Mason (1970), Carruthers & Grasso (1972), Coriell *et al.* (1977), Rodot, Bisch & Lasek (1979), Tagg *et al.* (1980), Bisch, Lasek & Rodot (1982), Elagin Lebedev & Tsmelev (1982), Sanz (1983), Sanz & Martinez (1983), among others. This experimental technique is very appropriate for hydrostatic studies. In the case of dynamic processes the presence of the outer liquid could modify the liquid bridge behaviour. However, available numerical results concerning non-rotating liquid bridges (Sanz 1983) show that the influence of the outer liquid on the volume of the drops resulting after liquid column breaking may be very small.

2. Mathematical model

In the following, unless otherwise stated, all physical quantities are made dimensionless using the characteristic length R, the radius of the disks, and the characteristic time $(\rho R^3/\sigma)^{\frac{1}{2}}$, ρ being the liquid density and σ the surface tension.

To calculate the evolution of the liquid bridge a one-dimensional inviscid slice

model (similar to the model used by Lee (1974) in capillary jet theory) has been used. This model can be deduced from the Euler equations by assuming the axial velocity W to be dependent upon the axial coordinate z and the time t but not upon the radial coordinate r. This one-dimensional model has been used also by Pimbley (1976) and Pimbley & Lee (1977) in the study of the breaking of capillary jets; by Cram (1983) in the study of the formation of droplets in welding processes, and by Meseguer (1983*a*,*b*), Meseguer *et al.* (1983), Sanz (1983) and Rivas & Meseguer (1984) in the analysis of liquid bridge dynamics. Details of numerical integration of the differential equations set can be found in Meseguer (1983*a*). In the slice model the radial momentum equation becomes decoupled, and the following equations of motion result:

Continuity equation

$$\frac{\partial S}{\partial t}+\frac{\partial Q}{\partial z}=0. \tag{2.1}$$

Axial momentum equation

$$\frac{\partial Q}{\partial t}+\frac{\partial}{\partial z}\left(\frac{Q^2}{S}\right)=-S\frac{\partial P}{\partial z}, \tag{2.2}$$

where the reduced pressure P, which accounts for both capillary and hydrostatic pressures, is given by

$$P=4\left[2S+\left(\frac{\partial S}{\partial z}\right)^2-S\frac{\partial^2 S}{\partial z^2}\right]\left[4S+\left(\frac{\partial S}{\partial z}\right)^2\right]^{-\frac{3}{2}}+Bo\cdot z. \tag{2.3}$$

In these expressions $S=F^2$ (where $r=F(z,t)$ stands for the equation of the interface shape) and $Q=WF^2$ are proportional to the cross-sectional area and the axial momentum of each slice, respectively. Bo is the static Bond number $Bo=\rho g R^2/\sigma$ where g is the acceleration due to microgravity. Boundary conditions are:

$$S(\pm A,t)=1, \quad Q(\pm A,t)=0, \tag{2.4}$$

where $A=L/2R$ is the slenderness. Initial conditions are:

$$S(z,0)=F_0^2(z), \quad Q(0,t)=0, \tag{2.5}$$

F_0 being the initial interface shape, which is related to the volume enclosed through

$$V=\pi\int_{-A}^{A}F_0^2(z)\,dz. \tag{2.6}$$

3. Equilibrium shapes

Equilibrium shapes are calculated in liquid bridge hydrostatics by solving (2.3) taking the reduced pressure P as constant along the liquid column. Equation (2.3) with $S(\pm A)=1$ is a two-point boundary problem with the additional complication that P is unknown and must be chosen to yield the correct liquid bridge volume. Equation (2.3) is usually solved as an initial-value problem (Coriell *et al.* 1977; Martinez 1978*a*) by guessing values of both P and the edge contact angle at one of the disks. In general, the values of the slenderness, the edge contact angle at the opposite disk and the liquid bridge volume obtained from the initial guess will not be the desired ones, and some iteration procedure must be adopted. In this paper we have tried a dynamic method to calculate liquid bridge equilibrium shapes in which boundary conditions at the disks are automatically met, and physical variables such as the slenderness and the volume are the problem input.

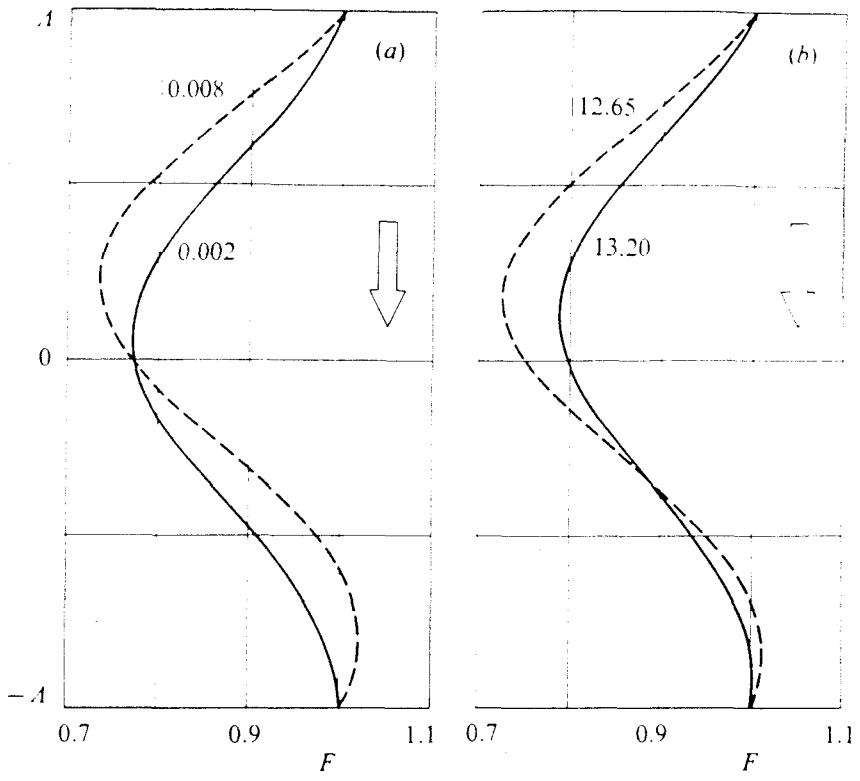

FIGURE 2. Equilibrium interface shapes of liquid bridges with a slenderness $\Lambda = 2.6$. The interface shapes in (*a*) correspond to liquid bridges with the same volume $V = 12.9$ subject to different Bond numbers, whereas those of (*b*) correspond to liquid bridges having different volumes subjected to the same Bond number $Bo = 0.005$. Numbers on the curves indicate the value of the Bond number in (*a*) and the volume in (*b*).

The basic idea may be explained in a few words: the slice model allows us to calculate the oscillatory motion around some equilibrium shape, provided the initial configuration lies in the stable region, so if some appropriate dissipative effect is introduced into the model the oscillation will be damped, and the process will tend to the equilibrium shape. To define the initial configuration the following expression for the interface shape has been taken:

$$S_0(z) = 1 + \left(\frac{V}{2\pi\Lambda} - 1\right)\left(1 + \cos\frac{\pi z}{\Lambda}\right) + 2Bo\left(z - \frac{\Lambda}{\sin\Lambda}\sin z\right), \tag{3.1}$$

and, to estimate the accuracy in calculating the equilibrium interface shapes, a parameter giving the maximum pressure difference along the liquid bridge has been introduced

$$\Delta P = (P_{\max} - P_{\min})/P_{\max}. \tag{3.2}$$

Let us assume that once the volume, the Bond number and the slenderness, and thence the interface shape as given by (3.1), are fixed, the evolution of the liquid bridge is calculated by using the slice model. The difference between capillary and hydrostatic (if it exists) pressure gradients generates a velocity field, and the liquid flows from the high- to the low-pressure regions. The interface shape changes, tending to smooth out the pressure distribution; since the liquid is assumed to be inviscid, when the configuration is close to equilibrium, the existing kinetic energy causes this position to be overpassed and the liquid bridge interface distorts in such a way that pressure gradients arise, tending to brake the movement. In consequence, if the initial configuration is stable, the liquid bridge will oscillate around some equilibrium interface shape. According to these considerations, the kinetic energy will be a

maximum when ΔP is a minimum; therefore, if at that moment the velocity field is cancelled, the resulting configuration will have less energy than the initial one, ΔP being closer to zero than at the starting time. Taking this last interface shape as the initial one of a new run, a third interface shape even closer to the equilibrium one will result, and so on. Calculations have been stopped when ΔP becomes smaller than a prefixed value which ranges from 0.005 at $A = 2.0$ to 0.001 at $A = 3.0$. Some of the calculated interface equilibrium shapes are shown in figure 2.

4. Stability limits and breaking process

The evolution of axisymmetric liquid bridges subject to a small axial gravity has been numerically studied for three values of the Bond number, $Bo = 0.01$, 0.005 and 0.002 (calculations have been performed on a Hewlett–Packard 9836 desktop computer using HP-PASCAL language).

Stability limits have been calculated as follows. Assume a liquid bridge having slenderness A and volume V in equilibrium under a Bond number Bi. Such a configuration, which is stable, is perturbed by increasing the Bond number from the initial value Bi to a new value $Bo > Bi$. If the perturbation $Bo - Bi$ is large enough the liquid bridge will break in two drops. The evolution of the liquid bridge interface is calculated by using the slice model, and the breaking time t_b (the time spent by the liquid bridge to reduce the neck radius from its initial value to zero) and the partial volume v_p (the larger drop volume to the whole liquid bridge volume ratio) are obtained.† The breaking time increases as the volume of the liquid bridge grows, as shown in figures 4 and 5, and becomes infinite at the critical value $V_m(A, Bi, Bo)$. For $V > V_m$ no breaking occurs: the liquid bridge under gravity given by Bo is stable for the initial condition Bi and the perturbation imposed (represented by $Bo - Bi$) and, thence, V_m is just the minimum-volume stability limit for the assumed values of A, Bi and Bo.

We discuss now the case $A = 2.6$ for which a large number of initial conditions have been considered. The results to be analysed are shown in the lower plot of figure 4 (the results obtained for $A = 3.0$, 2.3, 2.15 and 2.0 are plotted in figure 5). In figure 4, for each value of Bo, $V_m(A, Bi, Bo)$ decreases as Bi increases. The static minimum volume stability limit would be obtained by considering values of Bi as close as possible to the value of Bo, formally when $Bi = Bo$, which is numerically unattainable. To avoid this problem static stability limits have been calculated by extrapolation. In figure 6 the difference in volume $V_m(2.6, Bi, Bo) - V_m(2.6, 0, Bo)$ at two stability limits only distinguished by their initial conditions has been represented for three values of Bo. Two main aspects may be noted from figure 6: first that $V_m(A, Bi, Bo)$ varies almost linearly with Bi; and secondly that, for a given slenderness, the influence of initial conditions is the same no matter what the value of Bo is. In consequence, for other values of the slenderness it will be enough to determine this initial-conditions calibration curve, here performed by calculating at least three points of the curve (for example $V_m(A, 0, 0.01)$, $V_m(A, 0.005, 0.01)$ and $V_m(A, 0.008, 0.01)$), and one

† In the breaking process calculations are stopped when the neck radius becomes smaller than 0.1 because of numerical instabilities (spatial and time derivatives of both S and Q become very large in the neck region). At this point both the breaking time t_b and the partial volume v_p are well defined. In effect, as shown in figure 3 for a typical liquid bridge configuration, neck radius varies with time in such a way that when the stopping point is reached its slope is almost infinite. The slope of the curve giving the time variation of the volume of liquid enclosed between one of the disks and the neck bridge vanishes under the same condition and the value of v_p is clearly defined also.

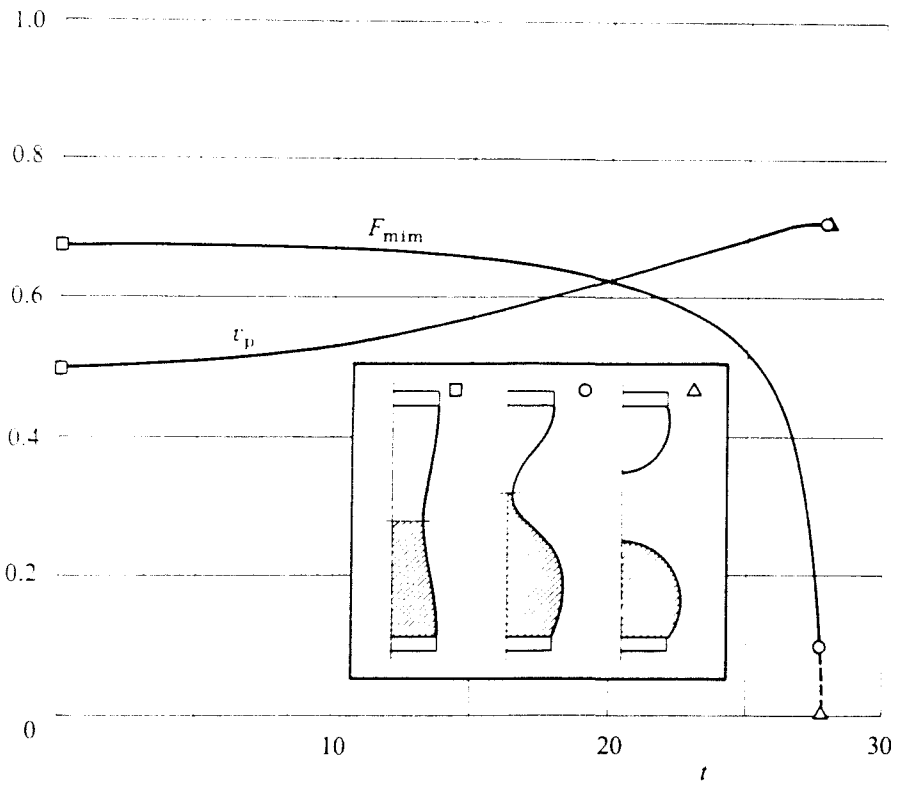

FIGURE 3. Variation with time t of neck radius F_{min} and partial volume v_p of a typical liquid bridge configuration ($A = 2.6$, $V = 11.9$, $Bi = 0$, $Bo = 0.002$). In this plot partial volume is defined as the larger fraction of the liquid bridge volume enclosed between the neck and one of the disks. The symbols indicate the interface shape as sketched in the insert.

representative point for the other two values of Bo (i.e. $V_m(A, 0, 0.002)$ and $V_m(A, 0, 0.005)$).

The partial volume v_p increases with liquid bridge volume V, but the rate of growth remains finite and even becomes smaller as V increases, in such a way that for a liquid bridge at the static stability limit (whose volume is $V_m(A, Bo, Bo)$) the partial volume is clearly defined. In table 1 the minimum volume stability limits and the partial volume at stability limits, resulting from figures 4 and 5, are summarized. In table 2 the static minimum volume stability limits are presented, these values being obtained by the extrapolation method explained above.

The influence of Bond number on the static minimum volume stability limits and the dependence on Bond number of the partial volume at these limits have been represented in figures 7 and 8, respectively. Liquid bridges become more sensitive to Bond number as A increases. To be able to produce a bridge with Bond numbers Bo from 0 to 0.01 the liquid bridge volume needs to be increased by over 3 % at $A = 2.15$, whereas the increase must be of 16 % at $A = 3.0$. Concerning v_p, the results are in accordance with those expected from experimental evidence. The volume of the larger drop resulting after breaking increases with the Bond number.

Additional conclusions concerning partial volume can be deduced from figures 4 and 5. These results corroborate the previous ones (Meseguer 1983*a*, *b*; Meseguer *et al.* 1983): v_p seems to be an intrinsic feature of liquid bridge breaking, depending mainly on both the slenderness of the bridge and on the volume of liquid enclosed, but not on the initial condition and breaking perturbation (Bi and $Bo - Bi$, respectively). This dependence is represented in figure 9, as the partial volume as a function of the liquid bridge volume for several values of A, which has been plotted from data presented in figures 7 and 8 (in figure 9, due to scale constraints, V_m/e^A

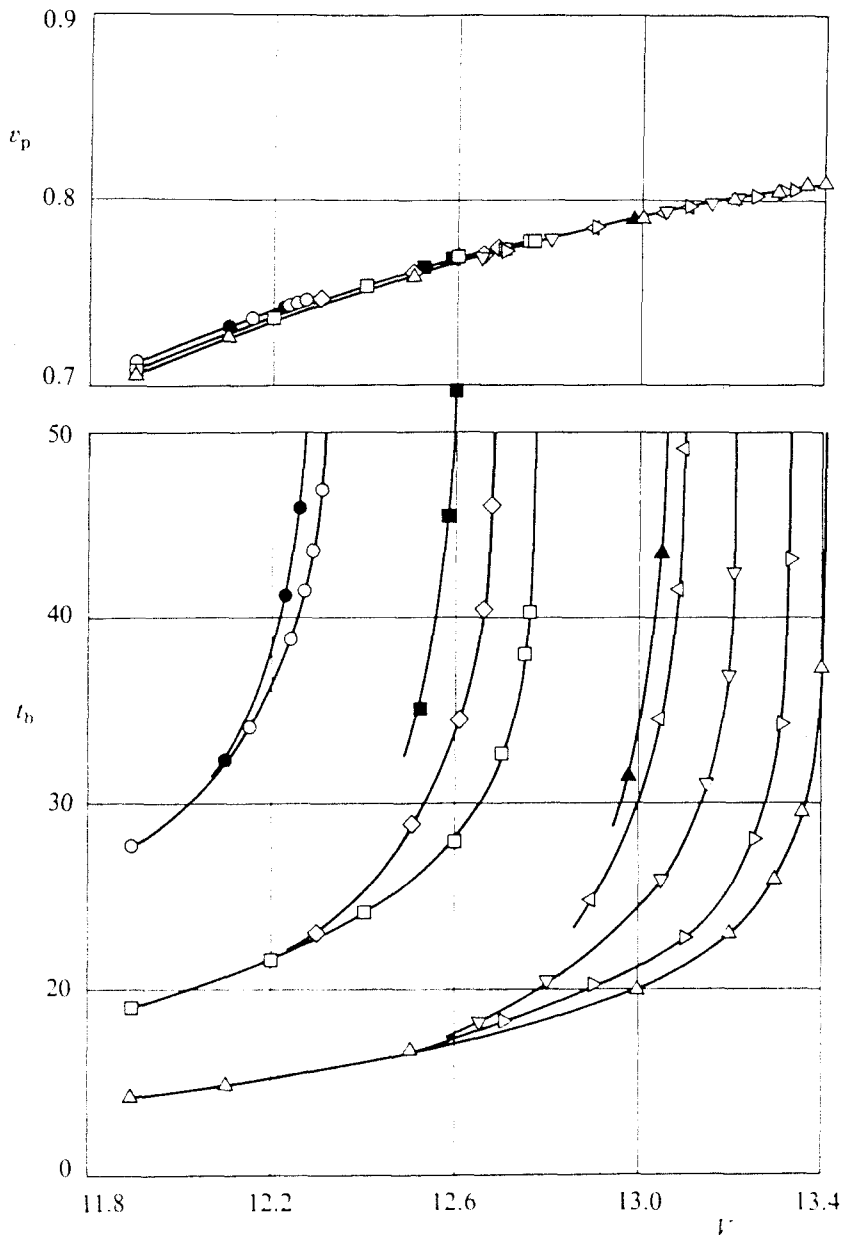

FIGURE 4. Partial volume v_p and breaking time t_b versus the volume V of liquid bridges with a slenderness $A = 2.6$. The symbols correspond to the cases numerically solved and indicate the values of initial conditions and breaking perturbations as in table 1.

has been plotted instead of V_m). According to this numerical analysis, if Bo is small enough, v_p depends mainly on easily controlled experimental variables such as the slenderness and the volume of the liquid bridge. This simplifies the method of correlating experimental and numerical results, and helps to validate the slice model for predicting the dynamic behaviour of liquid bridges.

Static results from this study are compared with those obtained by other investigators. The stability limit of cylindrical liquid bridges subject to axial microgravity has been studied in Meseguer (1983*b*), where the results from Carruthers & Grasso (1972), Coriell *et al.* (1977) and Vega & Perales (1983) are analysed. Some of these results (the variation with Bo of the maximum stable slenderness of cylindrical volume liquid bridges) are presented in table 3. As can be observed, the results obtained in Meseguer (1983*b*) give maximum stable slenderness below the values reported here. The difference arises because the previous results were calculated assuming that the liquid column was a cylinder at the initial time, which

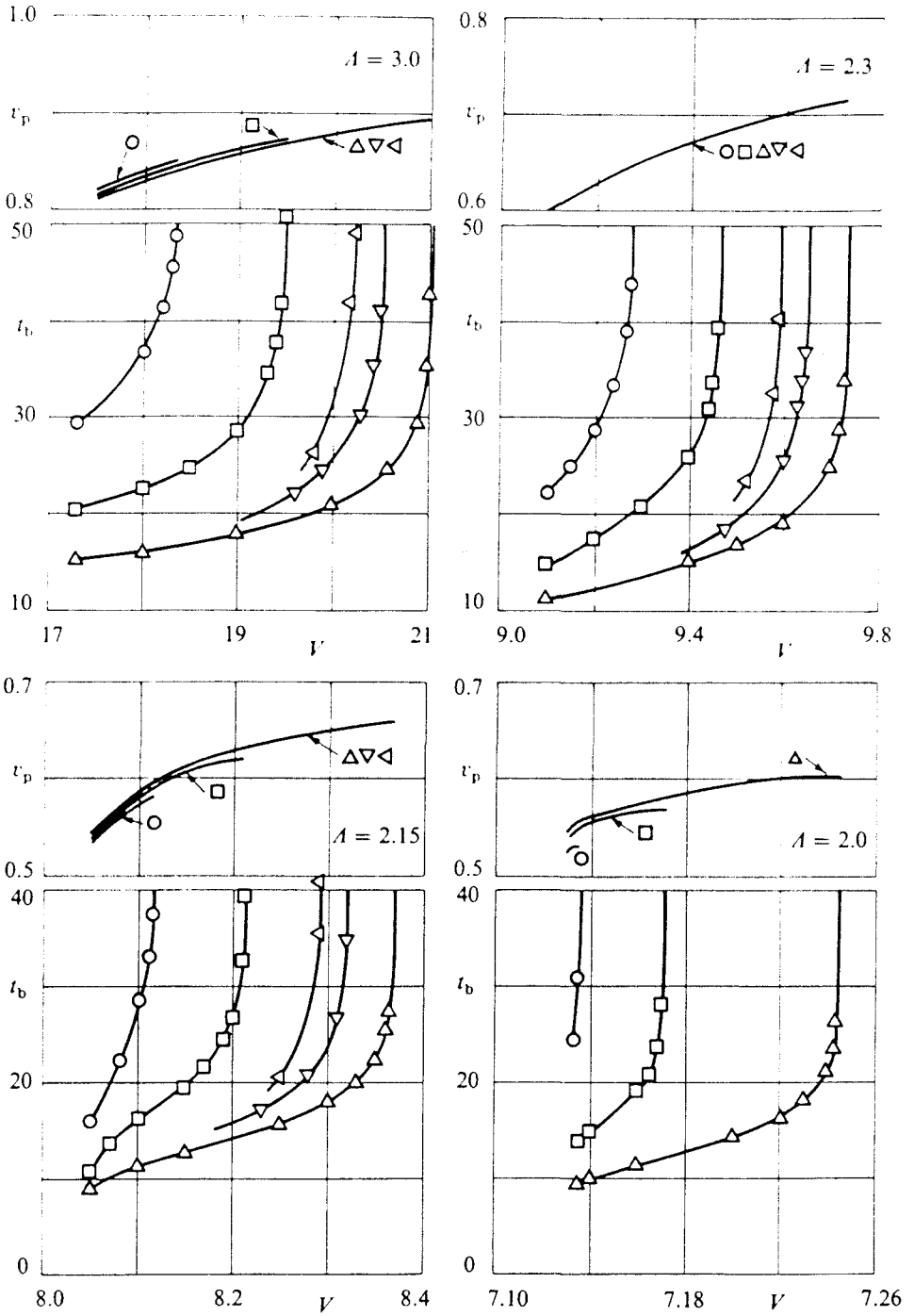

FIGURE 5. Partial volume v_p and breaking time t_b versus the volume V of liquid bridges with slenderness $\Lambda = 3.0, 2.3, 2.15$ and 2.0, respectively. The symbols correspond to the cases numerically solved and indicate the values of initial conditions and breaking perturbations as in table 1.

is the equilibrium shape corresponding to $Bi = 0$. Since the breaking perturbation increases with Bo, lower values of the maximum stable slenderness should be obtained, as shown here. The numerical results given in this paper agree with those of Coriell *et al.* (1977). Futhermore, an upper limit ($Bo = 0.005$) for the applicability of the results obtained by Vega & Perales (1983) through a perturbation analysis can also be established.

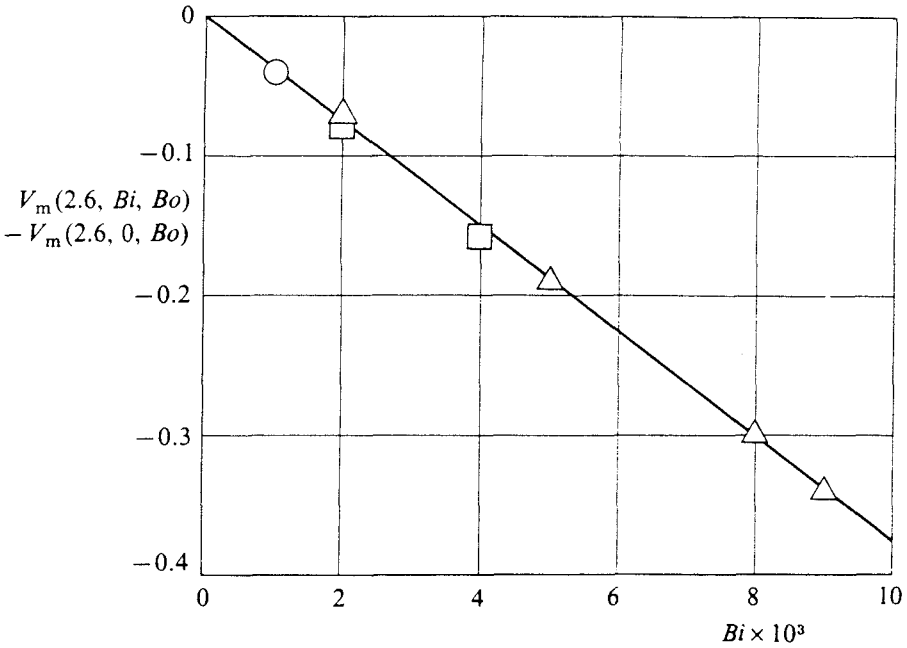

FIGURE 6. Variation of minimum volume stability limit $V_m(2.6, Bi, Bo) - V_m(2.6, 0, Bo)$ with initial conditions Bi for liquid bridges with a slenderness $A = 2.6$. The symbols indicate the values of Bond number Bo: △, 0.01; □, 0.005; ○, 0.002.

			$A = 3.0$		$A = 2.6$		$A = 2.3$		$A = 2.15$		$A = 2.0$	
Bo	Bi	SB	V_m	v_p	V_m	v_p	V_m	v_p	V_m	v_p	V_m	v_p
0.002	0.001	●	—	—	12.27	0.745	—	—	—	—	—	—
0.002	0	○	18.40	0.850	12.31	0.750	9.277	0.645	8.116	0.583	7.136	0.531
0.005	0.004	■	—	—	12.61	0.769	—	—	—	—	—	—
0.005	0.002	◇	—	—	12.69	0.774	—	—	—	—	—	—
0.005	0	□	19.51	0.872	12.77	0.778	9.460	0.681	8.215	0.621	7.171	0.564
0.010	0.009	▲	—	—	13.06	0.793	—	—	—	—	—	—
0.010	0.008	◁	20.25	0.883	13.11	0.796	9.594	0.699	8.296	0.646	—	—
0.010	0.005	△	20.54	0.887	13.22	0.801	9.648	0.706	8.320	0.651	—	—
0.010	0.002	▷	—	—	13.34	0.806	—	—	—	—	—	—
0.010	0	△	21.03	0.894	13.41	0.810	9.735	0.716	8.367	0.659	7.245	0.602

Bo, Bond number at breaking; Bi, Bond number used to calculate the initial-conditions equilibrium interface shapes; SB, symbols indicating the values of both Bo and Bi in figures 4 and 5; A, slenderness; V_m, minimum volume stability limit (made dimensionless with R^3) for the corresponding values of Bo and Bi; v_p, partial volume (defined as the ratio of the main drop volume to the whole liquid bridge volume) at the minimum volume stability limit.

TABLE 1

5. Apparatus

Experiments have been carried out in a Plateau tank (PT) already described in Martinez & Rivas (1982) which simulates the Fluid Physics Module (FPM) of the European Space Agency. A dimethyl silicone oil (Rhodorsil 47 V 20) with viscosity 20 times that of water and density $\rho = 954 \pm 0.5$ kg m^{-3} has been used as working liquid and a mixture of methanol and distilled water as the surrounding liquid. To improve interface visibility the dimethyl silicone oil was dyed slightly with yellow aniline.

	$Bo = 0$†		$Bo = 0.002$		$Bo = 0.005$		$Bo = 0.010$	
A	V_m	v_p	V_m	v_p	V_m	v_p	V_m	v_p
3.0	17.25	0.819	18.21	0.846	19.02	0.865	20.06	0.879
2.6	11.86	0.708	12.23	0.743	12.58	0.768	13.03	0.793
2.3	9.099	0.588	9.242	0.636	9.372	0.665	9.560	0.697
2.15	8.039	0.512	8.098	0.577	8.170	0.613	8.276	0.645
2.0	7.127	0.500	7.133	0.535	7.156	0.565	7.208	0.600

Bo, Bond number; A, slenderness; V_m, static minimum volume stability limit (made dimensionless with R^3); v_p, partial volume (defined as the ratio of the main drop volume to the whole liquid bridge volume) at the minimum volume stability limit. † In the case $Bo = 0$ the quoted values of V_m are from Martinez (1983) and that for v_p are from Meseguer *et al.* (1983).

TABLE 2

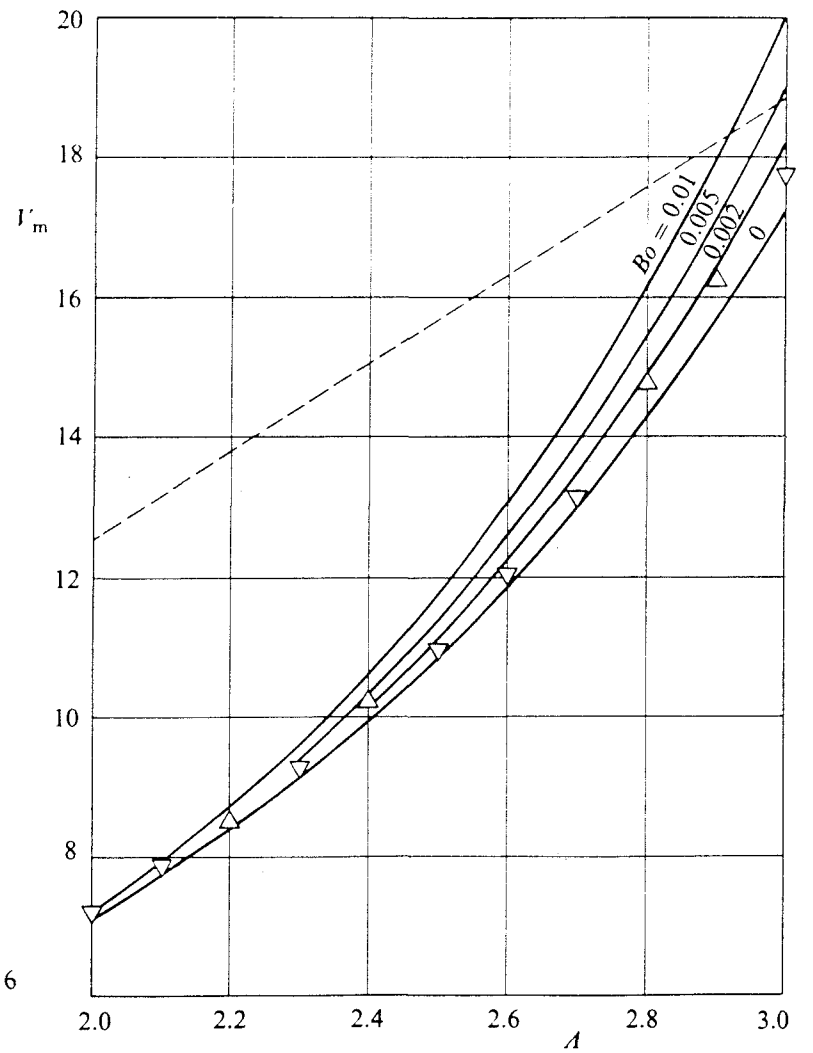

FIGURE 7. Static minimum volume stability limit V_m versus slenderness A for several values of the Bond number Bo. The dashed line corresponds to liquid bridge configurations having cylindrical volume $V = 2\pi A$. The symbols represent experimental results (volume of the liquid bridge at breaking) and indicate the value of the Bond number at breaking: ∇, $|Bo| \leqslant 0.005$; $\triangle$, $|Bo| > 0.005$.

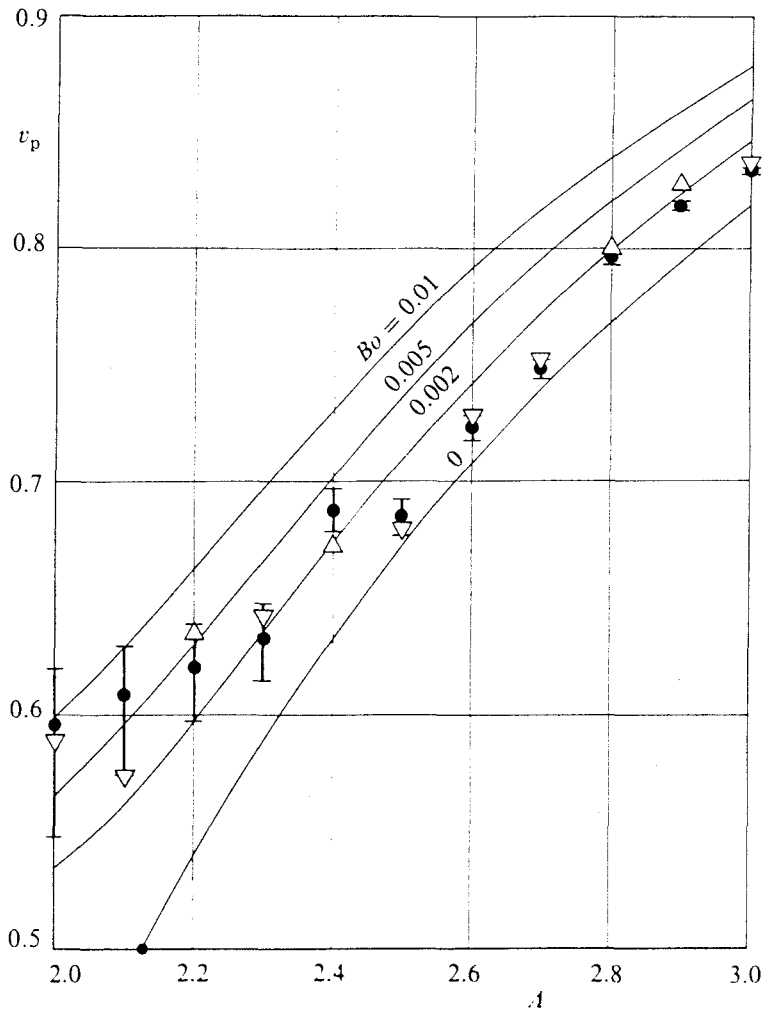

FIGURE 8. Partial volume at the minimum volume stability limit v_p versus slenderness A for several values of the Bond number Bo. The white symbols represent experimental results and indicate the value of the Bond number at breaking: ∇, $|Bo| \leqslant 0.005$; $\triangle$, $|Bo| > 0.005$; whereas the black symbols indicate the theoretical values of v_p corresponding to the different experimental liquid bridge configurations.

The tank, figure 10, is $140 \times 140 \times 60$ mm, with the sides made of 2 mm thick glass and the bottom of 10 mm thick Perspex. A removable plastic sheet minimizes methanol evaporation. The upper disk (the feeding disk), has two movements – rotation and axial displacement, and the bottom disk has three, namely, rotation, axial vibration and lateral displacement. Both disks are made of Perspex, in the shape of a frustrum cone, 15 mm radius, to provide sharp edges. The injection and removal of working fluid occurs through a 4 mm diameter hole in the centre of the upper disk. The working surface of the bottom disk is flat, whereas the working surface of the feeding disk presents a slight conicity to facilitate the evacuation through the injection hole of air bubbles trapped in the liquid bridge. Working-fluid injection and removal is made with a calibrated syringe, with the piston driven by a variable-speed electric motor. Liquid displaced by the piston passes through the filling duct, to which a three-way valve with a purge duct is connected. The purge duct is placed so as to trap air bubbles coming from the upper disk. The error in volume introduced by these air bubbles can be compensated for by measuring the change in height in the purge duct. The system was calibrated by using a burette with a precision of ± 0.2 cm^3, which can be taken as the precision of volume measurements.

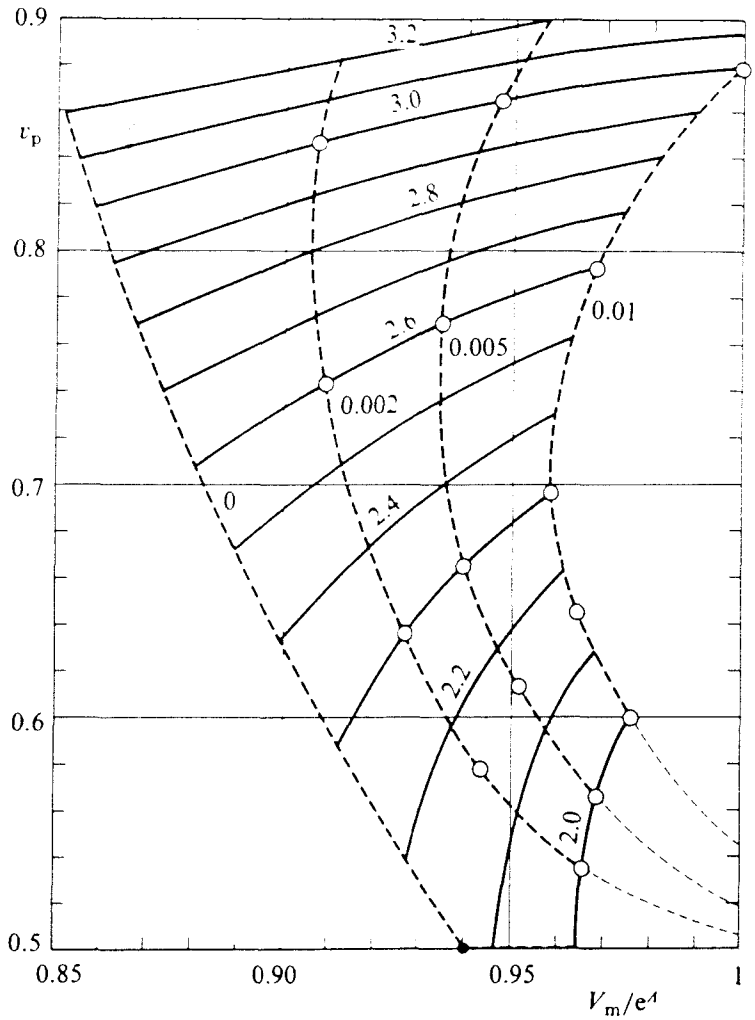

FIGURE 9. Partial volume v_p versus the static minimum volume stability limit V_m. The symbols correspond to the values obtained from the numerical analysis performed. Numbers on the curves indicate the values of the slenderness A (continuous lines) and the Bond number Bo (dashed lines).

	A_{cr}				
Bo	a	b	c	d	e
0.002	3.14	3.06	3.06	3.05	3.05
0.005	3.13	2.98	3.00	2.97	2.99
0.010	3.13	2.89	2.92	2.88	2.92

Bo, Bond number; A_{cr}, maximum stable slenderness of cylindrical volume liquid bridges for the corresponding Bond number. The values quoted are from (*a*) Carruthers & Grasso (1972); (*b*) Vega & Perales (1983); (*c*) Coriell *et al.* (1977); (*d*) Meseguer (1983*b*) and (*e*) calculated in this paper.

TABLE 3

The PT was not thermostated, but the temperature of the surrounding liquid was continuously measured using a thermometer with a precision of ± 0.1 °C. A magnetic stirrer at one side of the tank helped to keep uniform the temperature and alcohol composition. Background illumination consisted of a 60 W blue glass lamp with a 10 mm water filter 20 cm behind the rear glass of the tank. Very close to the rear face of the tank a translucent grid provided diffuse illumination and a reference frame for interface shape measurements (see figure 11). A photo-camera and a video-camera, 70 cm away, were used for image recording. A digital clock display was placed on the video-camera-viewed background for registration of the elapsed time.

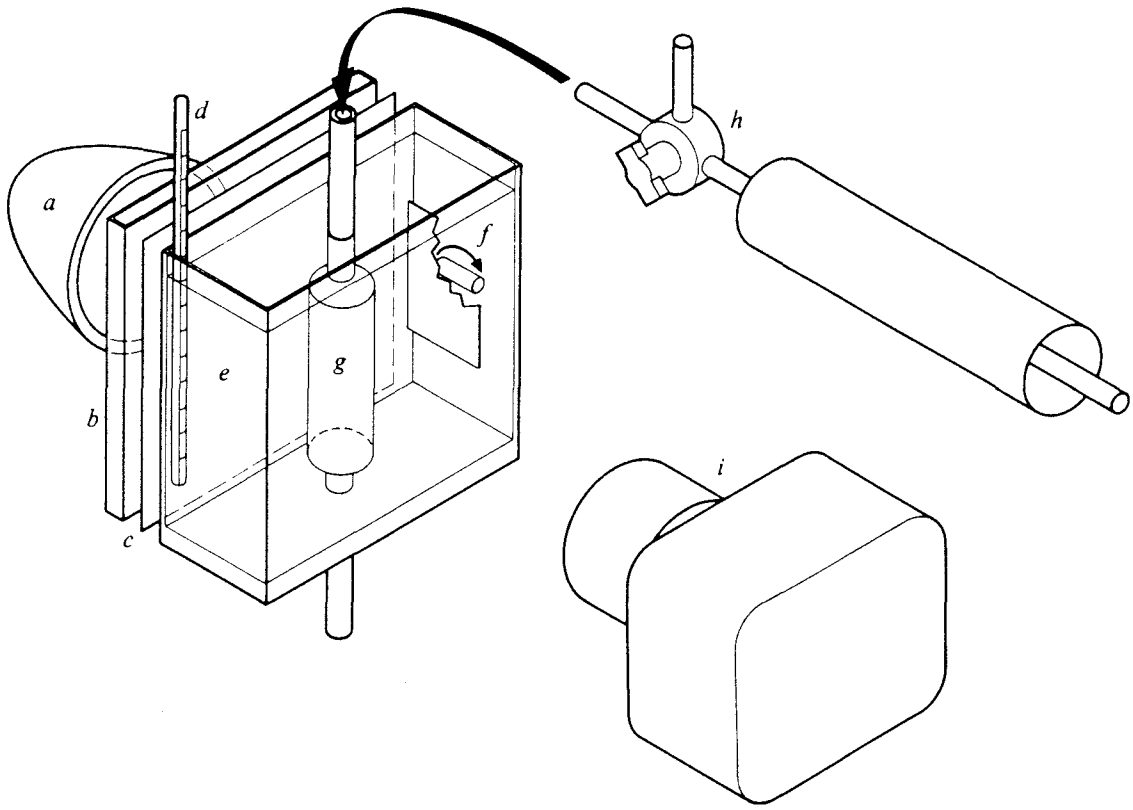

FIGURE 10. Experimental arrangement: (*a*) light source, (*b*) water filter, (*c*) translucent grid, (*d*) thermometer, (*e*) tank, (*f*) magnetic stirrer, (*g*) liquid bridge, (*h*) filling and purge system (*i*) image recording systems.

5.1. *Time variation of Bond number*

In PT experiments the Bond number is defined as $Bo = \Delta\rho g R^2/\sigma$, where $\Delta\rho$ is the difference between the liquid densities, g is the acceleration due to gravity, R the radius of the disks and σ the interfacial surface tension. Under these conditions density matching must be very accurate to obtain very small Bo values.

Methanol evaporation could not be completely avoided, and therefore an experiment was designed to measure the time variation of Bo. The same liquid bridge was used as a density indicator. In effect, to a first approximation, the equilibrium interface shape of a cylindrical liquid bridge subject to the action of an axial microgravity is (Meseguer 1983*b*)

$$F(z) = 1 + Bo\left(z - \frac{A}{\sin A}\sin z\right), \tag{5.1}$$

the maximum and the minimum liquid bridge radii, F_{max} and F_{min}, being reached at $z_m = \pm\cos^{-1}([\sin A]/A)$. In consequence, the Bond number is related to the liquid bridge deformation through

$$Bo = \frac{1}{2}\frac{F_{max} - F_{min}}{z_m - \dfrac{A}{\sin A}\sin z_m}. \tag{5.2}$$

It is assumed that Bo is positive ($Bo > 0$) when the liquid bridge is inside another liquid with an excess of methanol (the liquid bridge density is greater than the surrounding liquid density and the interface shape distorts, bulging out near the bottom disk and necking in at the upper), and negative ($Bo < 0$) when, due to methanol evaporation, the surrounding liquid density becomes greater than that of the liquid bridge (the interface shape is in opposition to that described above).

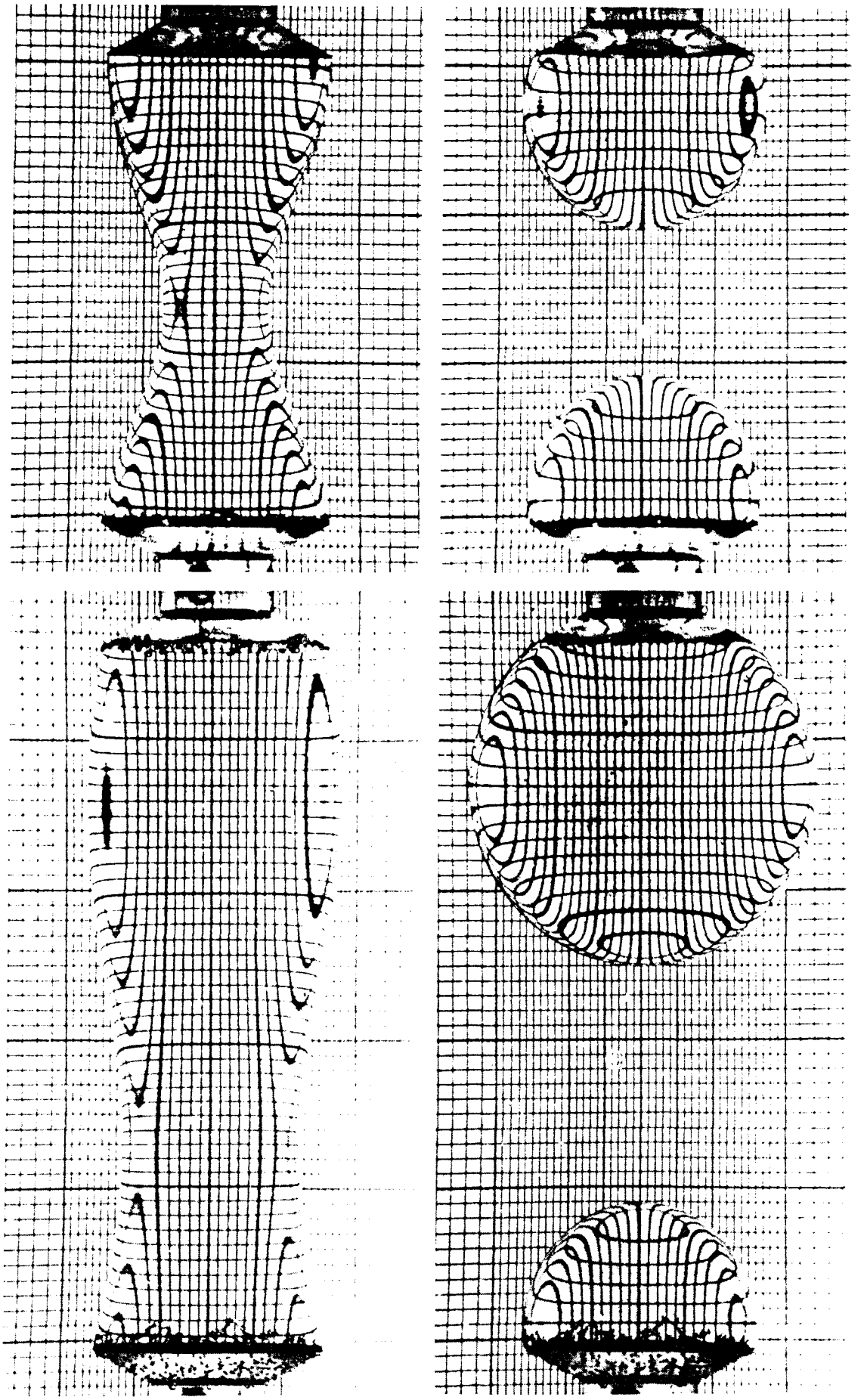

FIGURE 11. Photographs of liquid bridges, with slendernesses 2.0 and 3.0 respectively, before and after breaking, showing the magnifying-glass effect of the liquid column.

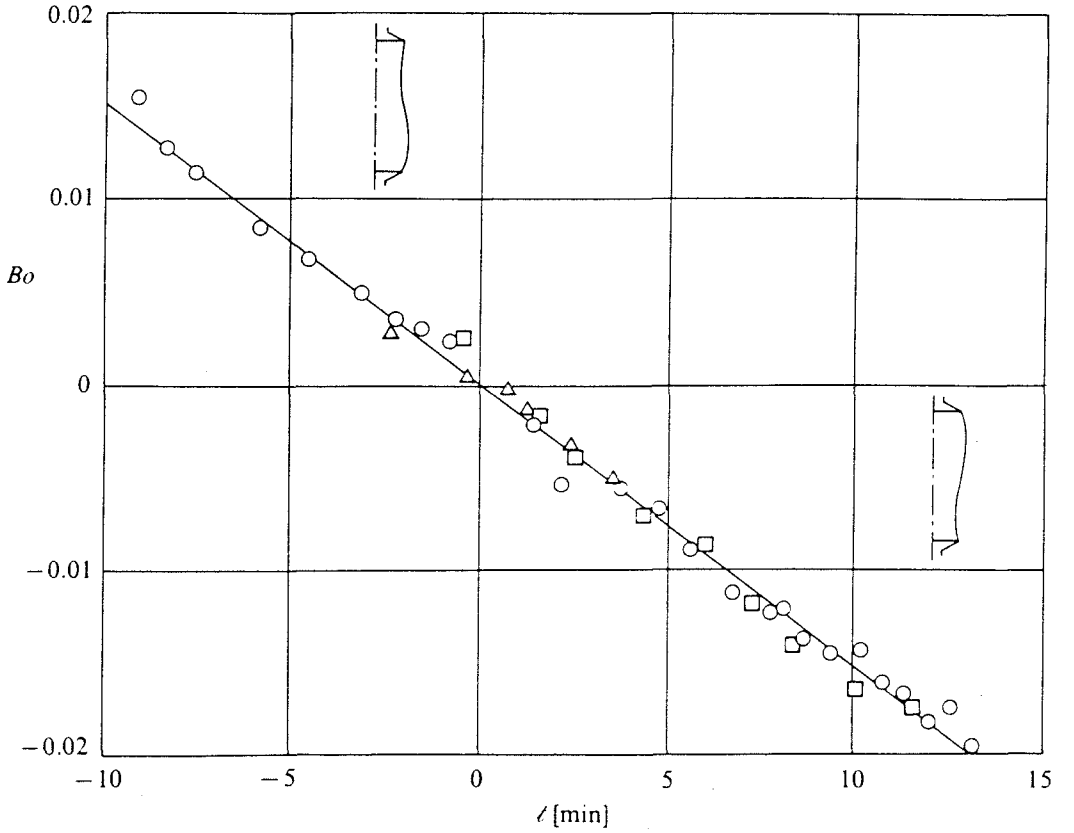

FIGURE 12. Variation of Bond number Bo with dimensional time ℓ. The symbols indicate the slenderness of the liquid bridge and the interval of temperatures during experiments: ○, 2.77, 23.7–24.1 °C; □, 2.77, 27.0–27.3 °C; △, 3.0, 26.6–26.7 °C.

Three calibration tests using cylindrical volume liquid bridges were performed, two of them at $A = 2.77$ and the third at $A = 3.0$. From time to time photographs of the liquid bridge interface were taken. F_{max} and F_{min} were measured from these pictures and Bo calculated from (5.2). The results obtained are plotted in figure 12. There is an almost linear dependence of Bond number with time, the rate of change being $dBo/d\ell = -1.53 \times 10^{-3}$ min^{-1}, ℓ being the dimensional time. A detailed study of this phenomenon can be found in Sanz (1983).

6. Experimental technique and results

At the beginning of all the experiments the surrounding liquid had methanol in excess, its density being slightly smaller than the liquid bridge density, aiming to provide a positive Bo (see figure 12) so that Bo was close to zero at the breaking time.

After density matching using a longer cylindrical column the desired slenderness and volume were fixed. The slenderness was reduced to the prefixed value, and some liquid was sucked from the bridge to maintain the cylindrical volume. Once A had been obtained, the liquid suction continued in two stages. Slow but continuous withdrawal of fluid brought the liquid bridge to the vicinity of the theoretical limit of minimum volume for $Bo = 0.01$ (obviously, this first stage is suppressed in the breaking at $A = 3.0$, see figure 7). Then very slow withdrawal occurred in steps of 0.5 cm^3, with settling in between each step to allow for interface instabilities, if any, to develop. Suction in this last stage must be performed at very low speeds to avoid significant velocity fields in the liquid bridge and to get breaking processes with initial conditions as close as possible to those stated in §2, the suction rate being smaller as A decreases.

Λ_i	Λ_b	$Bo_i \times 10^3$	$Bo_b \times 10^3$	$\ell_b - \ell_i$ [min]	$V \pm 0.06$	v_p	$\mathscr{T}_i, \mathscr{T}_b$ °C
2.77	2.0	14	−2	10.5	7.20	0.589	23.5, 23.8
2.77	2.1	14	−4	12.0	7.85	0.573	23.9, 24.3
2.77	2.2	10	−10	13.0	8.52	0.635	27.3, 27.4
2.77	2.3	10	2	5.0	9.23	0.642	25.6, 25.7
2.77	2.4	13	−10	15.3	10.23	0.672	23.5, 24.0
2.77	2.5	10	1	5.6	10.93	0.680	23.7, 23.8
2.77	2.6	22	−5	17.6	12.01	0.728	26.3, 26.8
3.0	2.7	6	−4	6.8	13.11	0.752	25.7, 25.8
3.0	2.8	1	−8	5.9	14.81	0.801	27.0, 27.2
3.0	2.9	−1	−6	3.0	16.29	0.828	27.3, 27.5
3.1	3.0	2	−2	2.7	17.73	0.837	26.1, 26.2

Λ, slenderness; Bo, Bond number; ℓ, dimensional time; V, volume of the liquid bridge at breaking (made dimensionless with R^3); v_p, partial volume, defined as the ratio of the main drop volume to the whole liquid bridge volume; $\mathscr{T}$, dimensional temperature. The subscripts i and b refer to starting time (density matching) and to breaking time respectively.

TABLE 4

In each run photographs were taken after the density matching, after every volume change step, and after the breakage takes place, the video-camera being used for recording the stepped withdrawal and the subsequent breaking process. The volume of the drops was calculated by numerical integration of the drop interface shapes from the pictures. To determine the interface shapes the grid placed at the rear face of the PT provided an accurate reference frame: pictures were enlarged and the diameter of the drops at each horizontal grid line as well as the distance between two reference vertical grid lines were measured. Then, taking into account both scale and conicity effects, the real diameters were calculated and from these last values the volume of the drops was obtained.

The experimental results are shown in table 4. For every experiment, the initial Bond number Bo_i refers to that determined from the density-matching picture (the zero time being reset at the instant that photograph was taken), and is calculated as explained in §5.1. The Bond number at breaking Bo_b is calculated from Bo_i and the measured time elapsed until the liquid bridge reaches its minimum volume stability limit, just before the breaking process accelerates, assuming the variation of Bond number with time to behave as in figure 12.

The control of Bond number seems to be the weak link in this set of experiments. In several experiments a bias has been introduced because of an optimistic estimation of the smallness of Bond number (and maybe because of a wrong estimation of the liquid bridge evolution rate, probably caused by the slowness of the beginning of the breaking process). Therefore, in some cases the liquid bridge volume has been excessively reduced. When, afterwards, Bo is calculated it is found that the liquid bridge has been forced to break with a volume less than that for the corresponding static minimum volume stability limit, as shown in figure 7, where experimental results giving the liquid bridge volume at breaking as a function of Λ are shown.

In figure 8 the experimental partial volumes v_p are plotted against Λ. Experimental and numerical results agree in the sense that v_p increases with Λ, although the influence on Bond number is not clearly indicated by experimental results for the reasons already stated: most of the experimental results correspond to liquid bridge configurations below the stability limit. In spite of this, since v_p is almost independent

of Bo (see figures 4 and 5), it is possible to calculate from figure 9 the partial volumes corresponding to experimental configurations. These numerical results are also plotted in figure 8. Although experimental values of the liquid bridge volume are given with an error of ± 0.06 (in dimensionless variables) which is constant for the whole range, the error in numerical partial volume increases as A decreases, as shown in figure 9. Numerical and experimental results are in agreement, except on a couple of points. The concordance is encouraging because, according to these experiments, the one-dimensional inviscid slice model accurately predicts the behaviour of axisymmetric liquid bridges, at least with respect to the aspects of the breaking problem treated in this paper.

7. Conclusions

The influence of the Bond number on the static minimum volume stability limit has been studied from a dynamic point of view by using a one-dimensional inviscid slice model. Additionally, this slice model has been used to calculate stable liquid bridge equilibrium shapes, providing a method of calculation in which the input variables are ones the experimentalist may easily control. These are the slenderness and the liquid bridge volume.

The influence of the slenderness, the volume, and the Bond number on the volume of the drops resulting after the liquid bridge breaking has been analysed. Numerical results show that partial volume depends mainly on the slenderness and on the whole of the liquid bridge, but not on the breaking perturbation. On the other hand, experimental results indicate that the one-dimensional slice model is very suitable for predicting the behaviour of axisymmetric slender liquid bridges, in spite of the simplifying hypotheses introduced in the theoretical model (the axial velocity is assumed to be constant over each slice and the radial momentum equation is not considered).

To conclude, it should be remembered that calculations are stopped before the neck radius vanished; in the subsequent evolution the liquid bridge splits in two drops (leaving apart satellite droplets) which remain anchored to the disks. This last part of the evolution has not been studied here, although some attempts in connection with this subject can be found in the literature. For instance, the work of Keller & Miksis (1983) could be a guide for study of the smoothing of the sharp apices appearing on the drops just after breakage. An estimation of the influence of microgravity on the final shape of these drops (which are spherical caps in the case $Bo = 0$) can be found in Chesters (1977).

This work has been supported by the Spanish National Commission for Space Research (CONIE) under a contract with the Polytechnic University of Madrid (UPM).

REFERENCES

Bisch, C., Lasek, A. & Rodot, H. 1982 Hydrodynamic behaviour of spherical semi-free liquid volumes in simulated weightlessness. *J. Méc. Théorique et Appliquée* **1**, 165–183.

Boucher, E. A. & Evans, M. J. B. 1980 Properties of fluid bridges between solids in a gravitational field. *J. Colloid Interface Sci.* **75**, 409–418.

Brown, R. A. & Scriven, L. E. 1980 The shapes and stability of captive rotating drops. *Phil. Trans. R. Soc. Lond.* A **297**, 51–79.

Carruthers, J. R. & Grasso, M. 1972 The stabilities of floating liquid zones in simulated zero gravity. *J. Cryst. Growth* **13/14**, 611–614.

CHESTERS, A. K. 1977 An analytical solution for the profile and volume of a small drop or bubble symmetrical about a vertical axis. *J. Fluid Mech.* **81**, 609–626.

CORIELL, S. R. & CORDES, M. R. 1977 Theory of molten zones shape and stability. *J. Cryst. Growth* **42**, 466–472.

CORIELL, S. R., HARDY, S. C. & CORDES, M. R. 1977 Stability of liquid zones. *J. Colloid Interface Sci.* **60**, 126–136.

CRAM, L. E. 1983 A numerical model of droplet formation. *CSIRO Div. Appl. Phys., Sydney, Australia* 2070.

DA RIVA, I. 1981 Stability of liquid bridges. In *Applications of Space Technology* (ed. L. G. Napolitano), pp. 69–80. Pergamon.

DA RIVA, I. & MANZANO, D. R. 1981 Impulsive motions of the floating zone. *PCH Physicochemical Hydrodynamics* **2**, 165–176.

DA RIVA, I. & MARTINEZ, I. 1979 Floating zone stability (Exp. 1-ES-331). In *Material Sciences in Space ESA* SP-142, pp. 67–73. Paris: ESA.

DA RIVA, I. & MESEGUER, J. 1978 On the structure of the floating zone in melting. *Acta Astronaut.* **5**, 637–653.

ELAGIN, M. P., LEBEDEV, A. P. & TSMELEV, A. V. 1982 Laboratory modeling of the stability and dynamics of free liquid zones. In *Hydromechanics and Heat and Mass Transfer in Zero-Gravity* (in Russian) (ed. V. S. Avduevskii & V. I. Polezhaev), pp. 24–33. Moscow: Nauka.

ERLE, M. A., GILLETTE, R. D. & DYSON, D. C. 1970 Stability of interfaces of revolution with constant surface tension. The case of catenoid. *Chem. Engng J.* **1**, 97–109.

GILLETTE, R. D. & DYSON, R. C. 1971 Stability of fluid interfaces of revolution between equal solid circular plates. *Chem. Engng J.* **2**, 44–54.

HARRIOT, G. M. & BROWN, R. A. 1983 Flow in a differentially rotated cylindrical drop at low Reynolds number. *J. Fluid Mech.* **126**, 269–285.

HAYNES, J. M. 1970 Stability of a fluid cylinder. *J. Colloid Interface Sci.* **32**, 652–654.

KELLER, J. B. & MIKSIS, M. J. 1983 Surface tension driven flows. *SIAM J. Appl. Maths* **43–2**, 268–277.

LEE, H. C. 1974 Drop formation in a liquid jet. *IBM J. Res. Dev.* **18**, 364–369.

MARTINEZ, I. 1976 Floating zone under reduced gravity. Axisymmetric equilibrium shapes. In *Material Sciences in Space ESA* SP-114, pp. 277–282. Paris: ESA.

MARTINEZ, I. 1978*a* Hidrostática de la zona flotante. Tesis doctoral, Universidad Politécnica de Madrid.

MARTINEZ, I. 1978*b* Floating zones. Equilibrium shapes and stability criteria. In *COSPAR: Space Research* Vol. XVIII (ed. M. J. Rycroft & A. C. Strickland), pp. 519–522. Pergamon.

MARTINEZ, I. 1983 Stability of axisymmetric liquid bridges. In *Material Sciences under Microgravity ESA* SP-191, pp. 267–273. Paris: ESA.

MARTINEZ, I. & RIVAS, D. 1982 Plateau Tank Facility for simulation of Spacelab experiments. *Acta Astronaut.* **9**, 339–342.

MASON, G. C. 1970 An experimental determination of the stable length of cylindrical liquid bubbles. *J. Colloid Interface Sci.* **32**, 172–176.

MESEGUER, J. 1983*a* The breaking of axisymmetric liquid bridges. *J. Fluid Mech.* **130**, 123–151.

MESEGUER, J. 1983*b* The influence of axial microgravity on the breakage of axisymmetric liquid bridges. *J. Cryst. Growth* **62**, 577–586.

MESEGUER, J. 1984 Stability of slender, axisymmetric liquid bridges between unequal disks. *J. Cryst. Growth* **67**, 141–143.

MESEGUER, J., SANZ, A. & RIVAS, D. 1983 The breaking of axisymmetric non-cylindrical liquid bridges. In *Materials Sciences under Microgravity ESA* SP-191, pp. 261–265. Paris: ESA.

PIMBLEY, W. T. 1976 Drop formation from a liquid jet: a linear one-dimensional analysis considered as a boundary value problem. *IBM J. Res. Dev.* **20**, 148–156.

PIMBLEY, W. T. & LEE, H. C. 1977 Satellite droplet formation in a liquid jet. *IBM J. Res. Dev.* **21**, 21–30.

RIVAS, D. & MESEGUER, J. 1984 One-dimensional, self-similar solution of the dynamics of axisymmetric slender liquid bridges. *J. Fluid Mech.* **138**, 417–429.

RODOT, H., BISCH, C. & LASEK, A. 1979 Zero gravity simulation of liquids in contact with a solid surface. *Acta Astronaut.* **6**, 1083–1092.

SANZ, A. 1983 Comportamiento de las zonas liquidas flotantes en microgravedad simulada. Tesis doctoral, Universidad Politécnica de Madrid.

SANZ, A. & MARTINEZ, I. 1983 Minimum volume for a liquid bridge between equal disks. *J. Colloid Interface Sci.* **93**, 235–240.

SLOBOZHANIN, L. A. 1982 Problems on the stability of liquids in equilibrium, appearing in spatial technology. In *Hydromechanics and Heat and Mass Transfer in Zero-Gravity* (in Russian) (ed. V. S. Avduevskii & V. I. Polezhaev), pp. 9–24. Moscow: Nauka.

TAGG, R., CAMMACK, L., CRONQUIST, A. & WANG, T. G. 1980 Rotating liquid drops: Plateau's experiment revisited. *JPL* 900–954, Jet Propulsion Laboratory, Caltech, Pasadena, California.

UNGAR, L. H. & BROWN, R. A. 1982 The dependence of the shape and stability of captive rotating drops on multiple parameters. *Phil. Trans. R. Soc. Lond.* A **306**, 347–370.

VEGA, J. M. & PERALES, J. M. 1983 Almost cylindrical isorotating liquid bridges for small Bond numbers. In *Materials Sciences under Microgravity ESA* SP-191, pp. 247–252. Paris: ESA.